IIETA International Information and Engineering Technology Association
Advancing the World of Information and Engineering

Journal of New Materials for Electrochemical Systems
Vol. 26, No.1, January 2023, pp.42-55
Journal homepage: http://iieta.org/journals/jnmes

Development of Molten Carbonate Fuel Cell Based on Lignin Fuel Consumption (MC-LFC): Correlation Between Modeling and Experimental Results

Ulrich L. Compaore[1*], Oumarou Savadogo[1] Mamadou L. Doumbia[2],

[1] Laboratory of New Materials for Energy and Electrochemistry-Chemical Engineering Department, Polytechnique Montréal
[2] Department of Electrical Engineering and Computer Engineering, the University of Quebec at Trois-Rivières

Corresponding Author Email: ulrich-landry.compaore@polymtl.ca ; osavadogo@polymtl.ca

https://doi.org/10.14447/jnmes.v26i1.a06

Received: August 02, 2022
Accepted: December 20, 2022

Keywords:
Direct Carbon Fuel cell (DCFC), lignin, Comsol, Butler-Volmer, porous electrode, transfer kinetic. Molten Carbonate Lignin Fuel Cell (MC-LFC), Performance

ABSTRACT

COMSOL software was used for the modeling of the performance parameters of the Molten Carbonate – Lignin Fuel Cell (MC-LFC), as it is a flexible tool, able to handle different physical approaches. The model developed includes the following processes: electronic and ionic charge balance (Ohm's law), Butler- Volmer charge transfer kinetics, diffusion gas flow in porous electrodes (Brinkman's equation), gas-phase mass balances in fuel and oxygen distribution channels, and porous electrodes (Maxwell-Stefan diffusion and convection). A parametric analysis was performed to evaluate the effect of material properties, pressure, and temperature, on cell performance. The results show that for a better performance of the MC-LFC cell, the exchange current density (A/m^2) in the anode and cathode compartment must be respected in the interval [0.075, 0.75] and [1.58, 15.8]. The electrical conductivity of the electrolyte (S/m), anodic and cathodic materials can be respectively in the interval [26, 265], [25, 250], and [19, 60]. It is also noted that the increase in temperature from 700 K to 1000 K generates a drop in the maximum power density of the battery (approximately 1500 mW/cm^2 to 1260 mW/cm^2). It is in every interest to operate the Cell MC-LFC under 500 °C.

NOMENCLATURE

C	concentration mol/m^3
S	surface, m^2
i	current density, $A.cm^{-2}$
R	gas constant, $J.mol^{-1}. K^{-1}$

1. INTRODUCTION

Nowadays, the availability of resources, the efficiency of production and utilization sources, and their environmental impacts are essential factors to be considered for the development of any energy system [1]. Fuel cells have the advantage of efficiently converting chemical energy into electrical energy without being limited by the theoretical efficiency of Carnot cycle [2]. Due to their conversion of energy they also have the merit of less polluting the environment [3]. Since the fuel cell was discovered by William Grove in 1839, a variety of fuel cells have been developed using gas (hydrogen, methane), liquid (methanol, ethanol), and solid (carbon) as fuel [4-10]. Hydrogen fuel cells have the particularity of being technically mature and are beginning to integrate more into the field of transport and stationary applications [11]. Nevertheless, researchers are increasingly focusing their attention on the carbon consumption fuel cell (DCFC) which has a theoretical energy efficiency of 100% and whose prototype was established by Jacques [12] more than 100 years ago. In 2007, Cao and al. [7] summarized the fundamental development of DCFC technology. In 2009, a review article by Cooper and Selman [13] explained the possible reaction mechanisms of carbon oxidation in molten carbonate fuel cells. In 2012, Giddey [14] summarized recent advances and technical challenges in DCFC technology, and discussed the future of this technology. After this article, Rady and his team [15] introduce different types of DCFC systems along with a discussion of the reaction mechanism. They focused on the properties of carbonaceous fuels and the analytical analysis techniques for applying a DCFC cell. Gür [16] provided a mechanistic insight into the different modes of solid fuel and oxygen delivery to the electrochemical reaction site using several DCFC system approaches. He also demonstrated the mechanism of carbon conversion to achieve efficient oxidation using a variety of DCFC systems on a fundamental basis [17]. Zhou and al. [18] summarized anode materials for DCFCs with the major challenge of fundamental understanding of materials science and engineering for the development of anodes. Cao and al. [19] gave a good overview of the evolution of DCFCs in recent years by discussing the fundamental understanding of the mechanisms and steps limiting the rate of carbon conversion. Despite these multiple efforts, the development of this technology remains relatively slow, with DCFCs facing difficulties in practical implementation in the choice of materials. It should be noted that the high resistance of the cell and the products formed during the reaction process with their structural and morphological changes are major drawbacks, resulting in unstable electrochemical power.

On the other hand, DCFCs are classified into three types according to the electrolyte used: molten hydroxide DCFC, molten carbonate DCFC, and solid oxide DCFC. The first type of DCFC cell was successful through demonstration by Scientific Applications and Research Associates Inc (SARA) operating the cell in a humid atmosphere. However, it is still necessary to improve the stability of the hydroxide caused by the high water concentration [20] for practical applications.

Compared to hydroxides, molten carbonates offer higher conductivity, a suitable melting temperature range (the operating temperature range), and a good degree of stability in atmospheres containing CO_2. Nevertheless, the oxidation of carbon at the anode is complex and constitutes a set of independent elementary reactions according to Cooper and Selman [13]. The third type of DCFC uses a solid electrolyte (YSZ, GDC) and is suitable for temperature operating conditions generally between 700 °C and 1000 °C [21]. Carbon oxidation is assumed to be the main reaction at the anode in a solid oxide DCFC but the addition of catalyst causes other reactions to become more dominant causing a drop in performance [21]. A recent DCFC cell design combining solid oxide and molten carbonate has been developed under the name hybrid direct carbon fuel cell (HDCFC). The authors reported higher power density than conventional DCFC batteries [22, 23]. However, the most experimentally studied DCFC prototypes to date are mostly powered continuously by fossil fuel [24-26]. More effort needs to be made to make DCFC system operate efficiently at low temperatures and consume bio-based carbon to limit environmental impacts. To consider the necessity to limit the negative environmental impact and to decrease the operating temperature of the system, we propose to develop a new concept a of cell which fits into the category of DCFCs named MC-LFC (molten carbonate-Lignin fuel cell) e.g. Molten Carbonate Fuel Cell based on lignin consumption).

The study and development of the MC-LFC begins with an analytical study which consists of determining the variation in voltage and the predicted output power of the battery as a function of the current (or current density). The voltage-current relationship can be the subject of a predictive study based on the theoretical characteristics of electrochemical processes (charge transfer and matter transport). The purpose of this article is to use COMSOL software to describe the predictable morphology of the power-current and voltage-current characteristics, considering the dependence of these on various physicochemical parameters (conductivity, porosity, diffusion coefficient) and operating conditions (temperature and pressure). Due to the complexity of the system, Modeling is one of the approaches which is necessary and useful to analyze or predict the behavior of the MC-LFC stack. However, any modeling may suffer from some limits which must be considered for the analysis of the results. Due to the approximations considered to facilitate calculations with COMSOL, the obtained results ability to predict stack performance, might be necessary limited. Thus, in a complementary way, we compared these calculated theoretical data to experimental results.

2. METHODS

2.1 Choice of MC-LFC stack components

We call it MC-LFC (Molten Carbonate Lignin Fuel Cell) and not DCFC (Direct Carbon Fuel Cell) because it is the molten lignin and carbonate which are used respectively as fuel and electrolyte for this cell concept. Thus, from the acronym MC-LFC the cell is directly classified according to the type of ionic conductor and the fuel used. Each component of the MC-LFC stack plays a very specific role and contributes in one way or another to the proper operation of the stack.

The electrolyte must have a high ionic conductivity and Molten salts in general exhibit this essential property; their composition and their nature can greatly contribute to reducing the parasitic effects affecting the performance of the cell such as the dissolution of the cathode material [27]. Studies [28, 29] have demonstrated that a eutectic mixture of molten carbonates allows an improvement in fluidity of the carbon inside the anode chamber and its transfer into the active electrochemical zone; where electro-oxidation reactions take place. Chunlin and his team [30] affirm experimentally that the addition of 5% by mass of Rb_2CO_3 or 5% by mass of Cs_2CO_3 lowers the melting point of carbonates (Li_2CO_3 -Na_2CO_3 -K_2CO_3) by 30°C. Kushashvili [24] used a ternary carbonate mixture with a composition of 43.4 mol% Li_2CO_3 , 31.2 mol% Na_2CO_3 and 25.4 mol% K_2CO_3 with 20 % additional Cs_2CO_3 and the cell performed well under an operating temperature of 700°C. Vutetakis [25] used a 32.1 Li_2CO_3 / 34.5 K_2CO_3 / 33.4 Na_2CO_3 ternary carbonate in a carbon-fired DCFC and was able to operate the cell at a temperature as low as 500 °C . All these studies are interesting because they show that the composition of the molten carbonate electrolyte is the important factor which makes it possible to reduce the operating temperature and to increase the stability of the cell. For decades, Janz and his team [31] reported a melting point temperature of 422°C of a molten carbonate mixture Li_2CO_3 -Na_2CO_3 -Cs_2CO_3 whose molar proportions are respectively 43.5%, 41.5% and 15% . In our analysis, the Li_2CO_3 -Na_2CO_3 -Cs_2CO_3 mixture is used as an ionic conductor in the same proportions as those of Janz. In conclusion, the use of molten carbonate has a number of advantages: it has good long-term stability with CO_2 gas [32], it can catalyze the oxidation of carbon [33] and it has an interesting ionic conductivity [34].

The anode support electro catalyst material must mainly act for this propose to facilitate rapid oxidation of the carbonaceous fuel. Nickel metal is generally used as the anode electro catalyst in the DCFC cell due to its high electrical conductivity (d~ 10^6 S/m), its ability to promote carbon oxidation and probably its relatively lower cost than platinum or vanadium. However, some researchers have investigated adding some additive to nickel to improve cell performance. Thus, by adding lanthanum strontium cobaltite ferrite(LSCF) which is a mixed ionic and electronic conductor to the nickel anode, Eun-kyung and Sin - Ae [35] were able to obtain a power density of 111 mW/cm ^{2} and therefore twice as high as nickel alone. W.Hao [36] and his team were able to obtain a power density of 156 mW/cm ^{2} by developing a DCFC cell with NiO-SDC(Samaria Doped Ceria) as the anode. Other researchers have studied the performance of a DCFC cell under a temperature above 600 °C using as anode materials NiO –YSZ (Yttria-Stabilized Zirconia) [37], CuO–ZnO– SDC [38], carbon microfibers (CMF) with NiO [39]. In this study, porous nickel is selected as material anodic.

The cathodic materials used must have high electronic conductivity, high mechanical strength and less soluble in molten salt. Nickel oxide is generally used because species (Li, Na…) from the molten salt electrolyte can be incorporated into the NiO crystal structure and create positive holes. It will thus be said that the conductivity of NiO depends strongly on the existence of defects in the crystal; it increases with the incorporation of species such as lithium in the nickel oxide [40]. Note, however, that some authors have used Ni-CeO_2 [41] or GDC (Gadolinium Doped Ceria) / LSCF (Lanthanum Strontium Cobaltite Ferrite) [42] as the cathode in the DCFC

stack operating at temperatures above 600 °C. Since nickel oxide is stable (low dissolution) in DCFC cell, then it is considered as cathode material for MC-LFC cell.

Various carbonaceous fuels have previously been used in the DCFC cell. These are graphite, carbon black, coal, petroleum coke, biomass (bamboo and waste paper [36], lignin [43], apple, sunflower, pine and willow, etc. Lignin in particular is considered one of the most viable biopolymers in the world, green carbon precursors [44] and abundant (about 50 million tons per year of lignin produced worldwide). In addition, it has a calorific value (i.e. 26.63 MJ/kg) [45] which makes it interesting for use as a reagent in the fuel cell (DLFC). In this work, substituting fossilized carbon (coal, hard coal, petroleum coke, etc.) generally used, until now in the DCFC fuel cell with lignin is an interesting and original choice of fuel for electrochemical energy production because the utilization of carbon from lignin is more sustainable than that of fossil fuels.

2.2 Proposal of a reaction mechanism for the MC-LFC stack

The use of lignin as fuel in a DCFC fuel cell can generate several types of gas (mainly CO_2, CO, H_2, H_2O) depending on the temperature (773 K - 1273 K) and operating pressure (1 atm – 30 atm). Considering a pressure and an operating temperature of the MC-LFC stack of 1 atm and 800 K, the gases likely to be released by chemical transformation are mainly H_2, H_2O, CH_4 and CO_2. Thus, lignin can be decomposed in the presence of molten carbonate according to the following reaction:

$$Lignine + (LiNaCs)_2CO_3 \rightarrow CO_2 + CH_4 + H_2 + H_2O + C \quad R1$$

From reaction R1, the following electrochemical reactions are proposed for the MC-LFC operating processes:

Anode reaction

$$C_{solide} + 2CO_3^{2-} \rightarrow 3CO_{2(g)} + 4e^- \quad \text{R2}$$

$$H_{2(g)} + CO_3^{2-} \rightarrow CO_{2(g)} + H_2O_{(g)} + 2e^- \quad \text{R3}$$

$$CH_4 + CO_{2(g)} \rightarrow 2H_{2(g)} + 2CO \quad \text{R4}$$

Cathode reaction

$$\frac{3}{2}O_{2(g)} + 3CO_{2_{(g)}} + 6e^- \rightarrow 3CO_3^{2-} \quad \text{R5}$$

If the CO_2 emitted in the anode compartment is totally consumed at the cathode, then the overall reaction is written:

$$C + \frac{3}{2}O_{2(g)} + CH_4 \rightarrow 2CO_{(g)} + H_{2(g)} + H_2O_{(g)} \quad \text{R6}$$

The equilibrium potential of the overall reaction noted E_T^0(i.e. 0.96 V) can be deduced according to the expression:

$$E_T^0 = -\Delta G_T^0/(6F) \quad (1)$$

where ΔG_T^0 is the Gibbs free energy at the temperature of 800 K and the pressure of 1atm whose value is equal to -560 kJ.

2.3 Configuration of the MC-LFC model with the Comsol software

At the anode, the lignin is first decomposed in the presence of molten carbonate to release gases (Reaction 1 or R1). Thereafter, an electro-chemical oxidation takes place, the carbon and the hydrogen react with the carbonate ions CO_3^{2-} to produce electrons which will circulate through the external circuit to the cathode. This is accompanied by a release of CO_2 gas at the anode (R2) if carbon is the fuel and water vapor plus CO_2 (R3). Finally, an endothermic chemical reaction ($\Delta H = 75$ kJ/mol) is observed which produces synthesis gases such as hydrogen and carbon monoxide (R4) due to the presence of methane and carbon dioxide as products of chemical reactions R1.

At the cathode oxygen reduction takes place where the oxygen molecules capture the oxidant CO_2 produced at the anode and the electrons arriving from the external circuit to regenerate the anions CO_3^{2-}. The reaction produces heat, and the excess non-recoverable CO_2 is released into the environment. Energy is then available at the terminals of the fuel cell and can be used to supply a load.

2.3.1 Description of model and parameters

Some parameters are set in accordance with the literature [52, 53] such as dynamic viscosity (mu) of gases, permeability and porosity (Shenzhen LS Tape Products Co., Ltd). The dimensions (length, width, and thickness) of the flow channel and the electrodes are arbitrarily chosen parameters. The conductivity, the molar fraction, the exchange current densities, the mass fractions, the concentrations of the chemical species and the effective diffusion coefficient of the species were the subject of calculation.

The mass fractions (w_k) of the chemical species involved in the oxidation-reduction reaction of the MC-LFC fuel cell are deduced from the formulation of Eq. 2 [51].

$$x_k = w_k \times \frac{M_{sum}}{M_k} \quad (2)$$

With M_k the molar mass of each of the components. The molar mass of the mixture M_{sum} is defined according to [25] by the following expression:

$$\frac{1}{M_{sum}} = \sum_{k=1}^{4} \frac{w_k}{M_k} \quad (3)$$

The molar fraction of each gaseous species (x_k)in the anode compartment was determined in a previous study using the equilib module of the factsage software.

Table 1. Mass fractions (w_k) of gases generated by decomposition of lignin in the anode, and cathode compartment

	Anode	cathode
H2	3%	-
CO	4%	-
H2O	36%	-
CH4	18%	-
CO2	38%	27%
O2	-	73%

The active specific surface (Sa) of the nickel anode and nickel oxide represents the small fraction of the structure of the electrodes, which is accessible to the reactive species and

this term is very important in the morphology of the electrodes and also influences strongly the resistance of the electrodes [54]. For the determination of the active surface, we considered the following approximation:

$$S_a = S_{a,a} = S_{a,c} = \rho_{electrode} \times A_s \quad (4)$$

With $\rho_{electrode}$ the density of porous nickel which is between 0.45~5 g/cm ^{3} and A_s the specific surface area given by the manufacturer which is approximately 18 m ^{2}/g.

Frank M. White [55] published the dynamic viscosity of some fluids whose main gases present in the MC-LFC stack are shown in table 2.

Table 2. Dynamic viscosity of gases at 20°C and 1 atm

Gaz	Dynamic viscosity [Pa.s]
H_2	9.05 x 10 $^{-6}$
H_2O	1.02x10 $^{-5}$
CO_2	1.48x10 $^{-5}$
CO	1.82 x 10 $^{-5}$
CH_4	1.34 x 10 $^{-5}$
O_2	2x10 $^{-5}$
air	1.8x10 $^{-5}$

Given that there is not a large variation in the dynamic viscosity of the gases according to Table 2, we assume that the dynamic viscosity of the fluids in the two compartments is of the order of 10^{-5}. It is known that the air of the terrestrial environment in the vicinity of the ground is a homogeneous gaseous mixture. It is approximately composed of nitrogen, oxygen, carbon dioxide, water vapor and traces of hydrogen. Given that these gas mixtures are found in the MC-LFC stack, we have considered that the viscosity of the air is approximately equal to the viscosity of the gas mixture in the two compartments to simplify the calculation of the fluid flow rates for solve Brinkman's equation. According to tables published by Frank M. White [55] on the thermo-physical properties of fluids, the dynamic viscosity of air (mu in Pa.s) can be expressed as a function of temperature by the following expression :

$$mu = 8{,}8 \times 10^{-15}T^3 - 3{,}2 \times 10^{-11}T^2 + 6{,}2 \times 10^{-8}T + 2{,}3 \times 10^{-6} \quad (5)$$

T is the temperature in Kelvin.

2.3.2 Secondary current distribution interface setting

The practical Butler-Volmer one electron charge -transfer model kinetics describe the charge transfer current density. Expression 6 describes a charge transfer reaction according to the complete Butler- Volmer equation , where the anodic and cathodic terms of the current density expression depend on the local concentrations of the electro-active species at the surface of the electrode [56, 57]:

$$i_{loc} = i_{0,a} C_R e^{(\alpha_a F \eta_{act})/RT} - i_{0,c} C_O e^{(-\alpha_c F \eta_{act})/RT} = i_{0,a} \frac{c_R}{c_{R-ref}} e^{(\alpha_a F \eta_{act})/RT} - i_{0,c} \frac{c_O}{c_{O-ref}} e^{(-\alpha_c F \eta_{act})/RT} \quad (6)$$

With C_R and C_O dimensionless terms, describing the dependence on the fraction of the reduced and oxidized species in the reaction in comparison to the initial species concentrations $C_{R\text{-}ref}$ and C_O-ref. The reference concentration of reductant R and oxidant O is calculated from Eq. (7).

$$c_{k\_ref} = \frac{c_{tot} \times (w_k/M_k)}{(\sum_{i=1}^{n} w_k/M_k)} \quad (7)$$

Where w_k and M_k are respectively the mass fraction and the molar mass of species k. Note that c_{tot} is the total molar concentration whose expression is established according to Eq. (8).

$$c_{tot} = \frac{P_{atm}}{R \times T} \quad (8)$$

It is assumed that the charge transfer kinetics equation leading to the calculation of the local anode current density in the case of the MC-LFC cell is the following [56, 57]:

$$i_a = i_{0,a} \left(\left(\frac{c_{CH4}}{c_{CH4,ref}} + \frac{c_C}{c_{C,ref}} \right) e^{(0,5F\eta)/RT} - \left(\frac{c_{CO}}{c_{CO,ref}} + \frac{c_{H2}}{c_{H2,ref}} + \frac{c_{H2O}}{c_{H2O,ref}} + \frac{c_{CO2}}{c_{CO2,ref}} \right) e^{(-1,5F\eta)/RT} \right) \quad (9)$$

Here $i_{0,a}$ is the anodic exchange current density (A/m^2), c_{CH4}, c_C, c_{CO}, c_{H2}, c_{H2O} and c_{CO2} are respectively the molar concentration of methane, carbon, carbon monoxide, hydrogen, and carbon dioxide (mol/m^3). $c_{CH4,ref}$, $c_{C,ref}$, $c_{CO,ref}$, $c_{H2,ref}$, $c_{H2O,ref}$ and c_{CO2} are the reference concentrations (mol/m^3). Moreover, F is the Faraday constant (C/mol), R the gas constant (J/(mol.K), T the temperature (K) and η the overvoltage (V). Thus, the current density (per unit volume) on the anode side is [57]:

$$j_a = S_{a,a} \times i_a \quad (10)$$

where $S_{a,a}$ is the active specific surface of the anode in m^{-1}. The active specific surface represents the small fraction of the structure of the electrodes, which is accessible to the reactive species and this term is one of the most important in the morphology of the electrodes and also strongly influences the resistance of the electrodes [54].

The exchange current density at the anode $(i_{0,a})$ is expressed according to the Arrhenius law [58] and can be written for the case of the MC-LFC cell as follows:

$$i_{0,a} = k_B e^{(-E_B/T)} = 6F k_f (\rho_C^S) e^{(-E_f/RT)} \quad (11)$$

To approximate the value of $i_{0,a}$ we use the expression of the exchange current density noted $i_{0,a1}$ from the work of Elleuch [58] expressed according to Eq. (12).

$$i_{0,a1} = k_B e^{(-E_B/T)} = 4F k_f (\rho_C^S) e^{(-E_f/RT)} \quad (12)$$

Where k_B and E_B are taken from work by [46] using pure carbon as fuel, Ni as anode material and a Li_2CO_3-Na_2CO_3-K_2CO_3 mixture as electrolyte.

By relating $i_{0,a}$ and $i_{0,a1}$ we get the following relationship:

$$\frac{i_{0,a}}{i_{0,a1}} = \frac{6F k_f (\rho_C^S) e^{(-E_f/RT)}}{4F k_f (\rho_C^S) e^{(-E_f/RT)}} \quad (13)$$

The value of $i_{0,a1}$ according to Elleuch [58] is equal to 0.005 A/m^2.

The charge transfer kinetics equation leading to calculate the local cathodic current density is the following [56, 57]:

$$i_c = i_{0,c}\left(e^{(3,5F\eta)/RT} - \left(\frac{c_{O2}}{c_{O2,ref}} + \frac{c_{CO2}}{c_{CO2,ref}}\right)e^{(-0,5F\eta)/RT}\right) \quad (14)$$

$i_{0,c}$ is the cathodic exchange current density (A/m^2).

Thus, the current density (per unit volume) on the cathode side is equal to:

$$j_c = S_{a,c} \times i_c \quad (15)$$

where $S_{a,c}$ represents the active specific surface of the cathode in m $^{-1}$.

To determine the exchange current density at the cathode, we based ourselves on the peroxide mechanism which can be used in our case [47, 59]:

$$i_{0,c} = i_{oc}^0 \times \left(P_{CO_2,c}\right)^{a_1} \times \left(P_{O_2,c}\right)^{a_2} \quad (16)$$

The values i_{oc}^0, a_1 and a_2 taken from [47]. Note that $P_{CO2,c}$, $P_{O2,c}$ are the partial pressures of the gases on the cathode side. Assuming that the total pressure at the entrance to the cathode compartment is equal to 1, then the relation linking the partial pressures of the gases can be summed up in Eq. (17):

$$P_{CO_2,c} + P_{O_2,c} = P_{cathode} = 1 \quad (17)$$

The partial pressures of CO_2 and O_2 are determined by solving Eq. (18) and Eq. (19) formulated from the Boudouard's reaction [60], and Eq. (17).

$$\left(P_{CO_2,c}\right)^2 - 2P_{CO_2,c} - k_{Boudouard} \times P_{CO_2,c} + 1 = 0 \quad (18)$$

$$\left(P_{O_2,c}\right)^2 - (2 + k_{Boudouard}) \times P_{O_2,c} + k_{Boudouard} = 0 \quad (19)$$

$k_{Boudouard}$ is Boudouard's constant previously defined by Hemme and Cassir [61]. This constant being a function of the temperature T can be established according to Eq. (20).

$$k_{Boudouard} = \frac{A}{T} + B \quad (20)$$

Using equation (20) Cassir [61] showed that the value of $k_{Boudouard}$ is 2,7 at 1000 K.

Where A (i.e. -15.279) and B (i.e. 16.61) are constants obtained using the table of values from [61, 62]under a temperature range of 800 K to 1275 K. From Eq. (19) and Eq. (20), the partial pressures of O_2 and CO_2 at the inlet of the cathode are calculated and the values are respectively 0.65 atm and 0.35 atm.

The reactions that occur in the MC-LFC battery can cause overvoltages (activation, ohmic and concentration) that must be evaluated. These losses decrease the battery voltage (V) with respect to its equilibrium potential (E) [63] according to the following expressions:

$$V_{cell} = \Delta E_{eq} - \eta_T = \Delta E_{eq,c} - \Delta E_{eq,a} - V_{pol} \quad (21)$$

$$\eta_T = \eta_{act,a} + \eta_{act,c} + \eta_{conc,a} + \eta_{conc,c} + \eta_{ohm} \quad (22)$$

Where V_{pol} is the polarization; η_{act} is the activation overvoltage; η_{conc} is the overvoltage due to mass transport and η_{ohm} is the ohmic overvoltage.

The equilibrium or ideal potential is given according to the NERNST equation as a function of the partial pressure of the gases present in the MC-LFC system:

$$\Delta E_{eq} = E_T^0 + \frac{RT}{6F} ln\left(\frac{P_C \times \left(P_{O_2,c}\right)^{3/2} \times P_{CH_4,a} \times \left(P_{CO_2,c}\right)^3}{\left(P_{CO,a}\right)^2 \times P_{H_2O,a} \times P_{H_2,a} \times \left(P_{CO_2,a}\right)^3}\right) \quad (23)$$

With all these data, the secondary current distribution interface of the COMSOL software was used for the generic modeling of the MC-LFC assuming that the electrolyte conducts current according to Ohm's law with constant conductivity. This distribution interface considers activation overvoltage, transfer of charged ions in the electrolyte (balance of charges in combination with Ohm's law), current conduction in the electrodes (Ohm's law). Additionally, it can be combined with the concentration-dependent current distribution (mass transport) interface in the COMSOL software. The potential at the anode input boundary is set to a reference potential of zero. At the cathode input boundary, the potential is set to the value of the cell voltage (V_{cell}). Thus, in this model, $\Delta E_{eq,a} = 0$ and $\Delta E_{eq,c} = 0{,}96V$. The simulation of the MC-LFC stack is performed over the range 0.16V < Vcell < 0.91 using Vpol in the range 0.05 V to 0.8 V as the parameter for the parametric solver.

2.3.3 Transport of concentrated species

The MC-LFC model describes a unit operating on lignin and an O_2/CO_2 mixture. At the anode, the lignin supplied as fuel decomposes into carbon and several gases (H_2, CH_4, CO, H_2O, and CO_2). In the cathode, the oxidants supplied are composed of oxygen, and carbon dioxide (coming from the anode). In the model we assume that diffusion dominates over electromigration then mass transport is described in COMSOL software by the Maxwell-Stefan diffusion and convection equations [64, 65], solved using a transport interface d concentrated species for each electrode flow compartment. Thus, the relative mass flux vector is defined as follows:

$$j_i = -\rho w_i \sum_{k=1}^{Q} \overline{D}_{ik} d_k - \frac{D_i^T}{T} \nabla T \quad (24)$$

Where $\overline{D}_{ik}$(m ^{2}/s) is the effective diffusion coefficient of species i and k, d_k (1/m) is the diffusion driving force, D_i^T(kg/m.s) is the thermal diffusion coefficient of species i.

The diffusion driving force [64, 65] is equal to:

$$d_k = \nabla x_k + \frac{1}{p}[(x_k - w_k)\nabla P] \quad (25)$$

The molar fraction (x_k) of each diffusing species is a function of the mass fraction (w) and the molar mass (M) of each of the components [51].

$$x_k = w_k \times \frac{M_{sum}}{M_k} \quad (26)$$

The molar mass of the mixture $M_{sum}$is defined according to [25] by the following expression:

$$\frac{1}{M_{sum}} = \sum_{k=1}^{4} \frac{w_k}{M_k} \quad (27)$$

The boundary conditions at the walls of the gas distribution channel and the electrodes are a zero-mass flux (insulation condition) expressed according to Eq. 28.

$$-nN\ i\ = n(\rho w_i u + j_i) = 0 \quad (28)$$

n is the normal unit pointing to the fluid domain.

At the entrance, the mass composition of the chemical species (O_2, CH_4, CO, H_2, H_2O, CO_2) is specified, while the exit condition is the convective flow. This assumption means that the convective term dominates the transport perpendicular to this boundary. Thus, we can write the condition of the outgoing flow as follows:

$$-n.\rho w_i \sum_{k=1}^{Q} \overline{D}_{ik} d_k = 0 \quad (29)$$

The overall diffusivity of binaries is evaluated using an empirical equation based on kinetic gas theory [66]:

$$D_{ik} = \frac{3{,}16.10^{-8} \times (T^{1,75}) \times \left(\frac{1}{M_i} + \frac{1}{M_k}\right)}{P \times \left(V_i^{1/3} + V_k^{1/3}\right)} \quad (30)$$

where M_i and M_k in kg/mol are the molar masses of the species, V_i, and V_k in m ^{3} /mol are the diffusion volumes of the gases.

We consider that the species transport occurs in a porous medium such as the nickel or porous nickel oxide electrode, this diffusivity matrix D_{ik} must be corrected by a factor F_e which is a function of the porosity and the tortuosity factor.

$$\begin{cases} F_e = \frac{\epsilon_p}{\tau_F} \\ \tau_F = \epsilon_P^{1/2} \end{cases} \quad (31)$$

ϵ_p and τ_F are respectively the porosity and the tortuosity of the porous electrode.

It is noted that the tortuosity factor explains the reduced diffusivity due to the fact that the solid grains prevent the Brownian motion and is determined according to the Bruggeman model [67].

2.3.4 Fluid flow in distribution channels and porous electrodes

In general, the flow in the distribution channels is governed by the Navier-Stokes equations using the steady-state form of continuity and conservation of momentum [68, 69]:

$$\nabla.(\rho u) = 0 \quad (32)$$

$$\rho(u.\nabla)u = \nabla.\left[-pI + \mu(\nabla u + (\nabla u)^{\mathrm{T}}) - \frac{2}{3}(\nabla.u)I\right] \quad (33a)$$

where u is the gas velocity in m/s, ρ is the gas density in kg/m^3, p is the pressure in Pa and μ is the dynamic viscosity of the gas in kg/m.s, T is the viscous stress tensor.

I is the interfacial viscous stress exchange which is related to the relative viscosity of the solid matrix and the liquid inclding the morphology of the porous martrix [68,69]

$$I = \frac{\mu}{\kappa}\, u \quad (33.b)$$

where u is the gas velocity in m/s, ρ is the gas density in kg/m^3, p is the pressure in Pa and μ is the dynamic viscosity of the gas in kg/m.s. The interfacial viscous stress exchange I in Eq.33.b corresponds to the microscopic momentum exchange of the Newtonian fluid with the solid matrix.

However, the Ni and NiO electrodes of the MC-LFC are porous layers, the Eq. (32) and Eq. (33a) change according to [68, 69] and become, respectively, Eq.34 and Eq.35 in the following form:

$$\nabla.(\rho u) = Q \quad (34)$$

$$\left(\frac{\mu}{\kappa} + Q\right)u = \nabla.\left[-pI + \frac{\mu}{\epsilon_p}(\nabla u + (\nabla u)^{\mathrm{T}}) - \frac{2}{3}\frac{\mu}{\epsilon_p}(\nabla.u)I\right] \quad (35)$$

Where κ is its permeability in m^{-2}. Eq. (35) is also known as Brinkman 's equation. Additionally, the permeability can be calculated using the Kozeny-Carman formula [70-72]:

$$\kappa = \frac{0{,}2.(\varepsilon^3)}{S_a(1-\varepsilon)^2} \quad (36)$$

S_a is the specific surface of the anodic or cathodic particles.

2.3.5 Determination of the ionic and electrical conductivity of cell components

The conductivity of the electrolyte is an essential property for the performance of fuel cells. This property has been measured at ambient pressure by many authors [49, 73, 74] particularly for calcium compositions [75, 76]. All are unanimous that the ionic conductivity of a ternary mixture of molten carbonate σ_{abc} is a function of temperature and obeys Arrhenius' law:

$$\sigma_{abc} = \sigma_{abc}^{0} e^{(-E_a/T)} \quad (37)$$

In the case of binary or ternary mixtures, the melting temperatures are lowered, and the stability domain of the liquid is wider. A quadratic activation law may then be more suitable to reproduce the experimental values [49, 73]. In this study, we estimated the electrical conductivity σ_{abc} (S/cm) of the molten carbonate mixture (with a=Li_2CO_3, b=Na_2CO_3 and c=Cs_2CO_3) from the equivalent electrical conductivity Λ_{abc}(S cm^2 equiv^{-1}) and the molar volume of the mixture noted V_{abc} (cm^3.mol^{-1}) according to the following formulation:

$$\sigma_{abc} = \frac{\Lambda_{abc}}{V_{abc}} \quad (38)$$

The molar volume (V_{abc}) of the ternary mixture (43.5:41.5:15 mol% of Li_2CO_3, Na_2CO_3 and Cs_2CO_3) is expressed according to the following relationship:

$$V_{abc} = \sum_{i=a}^{c} x_i V_i = \frac{\sum_{i=a}^{c} x_i M_i}{\rho_{electrolyte}} \quad (39)$$

Where Mi and X_i are respectively the molar mass and the molar fraction of the pure components (Li_2CO_3, Na_2CO_3 and Cs_2CO_3). $\rho_{electrolyte}$ is the density of the ternary mixture

(g.cm $^{-3}$) expressed according to [51]. According to Kojima [49], the equivalent conductivity can be written as:

$$\Lambda_{abc} = \frac{1}{3}(\Lambda_{a-bc} + \Lambda_{b-ca} + \Lambda_{c-ab}) \quad (40)$$

It is admitted that the expressions of Λ_{a-bc}, Λ_{b-ca}, and Λ_{c-ab} of Eq. (40) can be established based on the general formula of the equivalent conductivity of the bits.

$$\Lambda_{a-bc} = x_a\Lambda_a + x_{bc}\Lambda_{b-c} - x_a x_{bc} k_{carbonate}|r_{bc} - r_a| \times \left(\frac{x_a\Lambda_a}{r_a} + \frac{x_{bc}\Lambda_{b-c}}{r_{bc}}\right) \quad (41)$$

$$\Lambda_{b-ca} = x_b\Lambda_b + x_{ca}\Lambda_{c-a} - x_b x_{ca} k_{carbonate}|r_{ca} - r_b| \times \left(\frac{x_b\Lambda_b}{r_b} + \frac{x_{ca}\Lambda_{c-a}}{r_{ca}}\right) \quad (42)$$

$$\Lambda_{c-ab} = x_c\Lambda_c + x_{ab}\Lambda_{a-b} - x_c x_{ab} k_{carbonate}|r_{ab} - r_c| \times \left(\frac{x_c\Lambda_c}{r_c} + \frac{x_{ab}\Lambda_{a-b}}{r_{ab}}\right) \quad (43)$$

x_a , x_b and x_c are the molar fractions of the pure components Li_2CO_3 , Na_2CO_3 and Cs_2CO_3; Λ_a, Λ_b, Λ_c, are the equivalent conductivities of the pure components Li_2CO_3 , Na_2CO_3 and Cs_2CO_3; Λ_{b-c}, Λ_{c-a} and Λ_{a-b} are respectively the equivalent conductivities of the binary mixture of Na_2CO_3 - Cs_2CO_3 , Cs_2CO_3 -Li_2CO_3 and Li_2CO_3 -Na_2CO_3 ; r_a, r_b and r_c are ionic radii (Å) respectively Li_2CO_3 , Na_2CO_3 and Cs_2CO_3 ; $k_{carbonate}$ is a constant at a given temperature obtained by adjustment from the work of [77] whose expression is described in Eq. (44).

$$k_{carbonate} = 4{,}381 - 2{,}099 \times 10^{-3}\, T \quad (44)$$

$$r_{bc} = (1 - x_c)r_b + x_c r_c \quad (45)$$

For a binary mixture of molten carbonate Kojima and al [78] demonstrated that the equivalent conductivity of the binaries can be written as follows:

$$\Lambda_{b-c} = x_a\Lambda_a + x_b\Lambda_b - x_a x_b k_{carbonate}|r_b - r_a| \times \left(\frac{x_a\Lambda_a}{r_a} + \frac{x_b\Lambda_b}{r_b}\right) \quad (46)$$

Knowing the equivalent conductivity and the molar volume of the ternary mixture, the value of the conductivity of the electrolyte used in the MC-LFC cell is calculated.

The electrical conductivity of NiO has been measured in air and formulated by Tare and Wagner [48] according to Eq. (47):

$$log(\sigma_{NiO}) = 2{,}774 \pm 0{,}07 - \frac{3460 \pm 80}{T} = kseff\_c \quad (47)$$

The electrical conductivity of Ni is determined from Eq. (48).

$$\sigma_{Ni} = \frac{1}{\rho_{Ni}} = kseff\_a \quad (48)$$

Where ρ_{Ni} represents the resistivity of nickel. In the case of metallic crystals, resistivity increases linearly with temperature; this is due to the interaction between electrons and phonons. Since the operating temperature of the cell does not vary too much, the resistivity of nickel at a temperature T can be expressed by linear approximation: according to Eq. (49).

$$\rho_{Ni} = \rho_0\big(1 + \alpha_0(T - T_0)\big) \quad (49)$$

with T_0 the reference temperature in (°C), $\rho_0$the resistivity at temperature T_0 (Ω.m); α_0 the temperature coefficient at the temperature T_0 (°C^{-1}) and T the temperature in (°C).

3. RESULTS AND DISCUSSION

3.1 MC-LFC performance

We present some results of the simulation which are compared to those of existing studies whose anchor point is the study of the performance of DCFC.

By maintaining an anode exchange current density of 0.75 A/m^2, a temperature of 500°C and a pressure of 1 atm, the maximum and optimum power of the cell obtained by modeling is respectively 2380 W/m^2 and 1950 W/m^2 (Fig. 1); this confirms that the efficiency of the MC-LFC is 82%. The optimum voltage is 0.72 V. Then the overall overvoltage would be 0.24 V; this value is high, because it is clearly greater than 0.06 V (obtained by calculating the ratio between the product of the ideal gas constant and the temperature by the Faraday constant RT/F).

The simulation results of this work show that if we want to minimize the global overvoltage, it would be necessary to increase the rate constants for the transport of matter (variations in the concentration of species in the electrolyte solution) and for the transport of charge (application to the electrode of an over-potential to quickly activate the electrochemical reaction). It is also possible to increase the roughness of the electrodes finally to increase their surface and adopt a design from the practical point of view which will make it possible to minimize the contact resistance at the level of the interconnections.

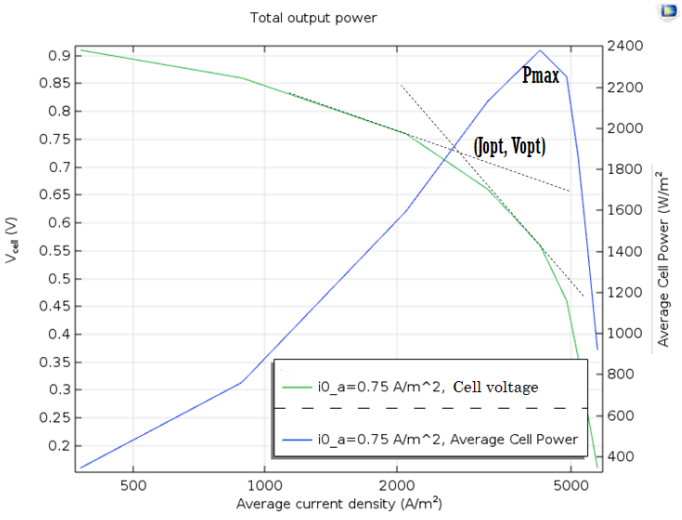

Figure 1. Curve of voltage (green) and power density (blue) as a function of current density of the MC-LFC stack under an operating temperature of 800 K.

According to table 3, the performance of a DCFC depends on several factors such as the temperature, the nature of the fuel and the type of materials used for electronic and ionic conductors

Table 3. Comparison of the performance of different DCFC cells obtained experimentally compared to the MC-LFC modeled with COMSOL software.

Anode	Cathode	Electrolyte	Puissance (W/m^2)	T (°C)	Ref
lignin + Charcoal activated	catalytic compounds	SDC –(Li/Na) $2CO_3$ composite	250	560	[4]
NiO - SDC	LSCF	SDC	680 - 2250	650	[36]
3D NiO -GDC	$Sm_{0.5}$ $Sr_{0.5}$ CoO_3	$Ce_{0.8}Gd_{0.2}O_{1.95}$ (GDC) – carbonate composite	1430	500	[6]
Ni	NiO	Molten carbonate	1390	525	
Ni	NiO	Li_2CO_3/Na_2CO_3	1000	650	[79]
Ag-GDC	Ag-GDC	YSZ + Al_2O_3	2210	850	[10]

By comparing the performance curve of the MC-LFC modeled on the COMSOL software obtained in this work with the experimental studies of Raquel and her team [4]. In the first time study of the authors of reference [4], the two types of lignin used in their commercial forms where respectively Lignosulfonate (LS) and Kraft lignin (KL). Prior to their utilisation, they were blended with commercial active carbon (AC) or after alterning their structure by changing the pH to 10. They claim that addition of the active carbon (AC) increased the current density from from 43–57 to 83–101 mA cm−2. And KL+ AC based lignin exhibits a typical power density of 12 $mW.cm^{-2}$ whereas the typical power density of the lognin based on LS + AC was and 25 mW cm^{-2} ((i.e. a current density of 80 mA/cm^2 and a voltage of 0.31 V at 833 K). This is 2 times higer than that of KL +AC. This is a large variation in the power density. There is indeed a considerable drop in the operating voltage. This shows that the overall overvoltage of the cell is very high (> 0.60 V) and is probably due to the choice of materials which exert an influence on the transport of the electro-active species of the cell. Then, by comparing the performance of the c MC-LFC obtained with COMSOL to the SOFC cell obtained experimentally by H. Wu and al [10], it is found that the last one has a much better power density (ie 2210 W/m^2 against 1390 W/m^2). However, the operating temperature is higher (850 °C for the SOFC compared to 525 °C for the MC-LFC) and the materials used are expensive. The direct DCFC [6] demonstrates that it is possible to have good performance for DCFC systems operating at a temperature of 500 °C using catalytic materials ($Sm_{0.5}Sr_{0.5}CoO_3$, GDC, etc. to facilitate the oxidation of carbon and the reduction of oxygen. They were able to obtain a power density of 1430 W/m^2 slightly higher than that of the MC-LFC. J. Rosen and al [79] developed a molten carbonate fuel cell (MCFC) using the same electrode materials as the MC-LFC cell but has a lower maximum power density than the cell modeled in this study. It is also important to point out that the experimental power density obtained in reference [4] is almost one order of magnitude lower that the values obtained from simulations. The differences in performances obtained from the different simulations and the experimental results are related to the fuel and the composition of the molten salt used, their impurities and the real electro catalytic properties of the electrode materials. Although simulation can optimize the conductivity of the electrolyte and the electrodes, the difference between experimental and simulation results is an indication that it is more difficult to simulate the behavior of electrocatalytic reactions in a such complex systems. This is also an indication that it is, of course, to optimize other cell parameters and not only the electrolyte conductivity if we want to improve the performance of the MC-LFC. Effectively, The performance of the cell depends on various parameters as the temperature, the operating pressure, the physico-chemical properties of the electrode materials, the electro-catalytic parameters of the reactions, the electrolyte and the fuel used to operate the cell. Therefore, it is necessary to carry out a parametric analysis of the effect of each of these different operating parameters that can affect the performance of the MC-LFC stack. This will help to better understand the limits of such a system and to determine the limiting parameter on the cell performances.

3.1 Parametric studie

Parametric studies were carried out by modifying certain variables according to the condition limits of the modeling process. Accordingly, the effect of the following several parameters on the performances of MC-LFC stack was evaluated: the ionic conductivity of the electrolyte, the electrical conductivity of the anode and the cathode layers (Fig. 2, Fig. 3, Fig. 4), the cell operating temperature and pressure; and, respectively, the exchange current density of the anode and the cathode reactions (Fig. 5, Fig.6, Fig.7, and Fig.8).

Fig. 2 shows the simulated curves of the effect of the ionic conductivity of the electrolyte on the power density of the MC-LFC. The decrease in ionic conductivity from 265 S/m to 0.265 S/m or 3 orders of magnitude, leads to poorer performance of the MC-LFC cell. The average optimum power density is almost 1400 $W.m^{-2}$ for an ionic conductivity of 265 S/m whereas it is 400 W. m^{-2} for the electrolyte ionic conductivity of 0.265 S/m. For a 1000 times decrease of the conductivity, the power density decreases by only 3.5 times. Furthermore, the increase of the ionic conductivity from 0.265 S/m to 26,5 S/m or 2 orders of magnitudes increases the conductivity from 400 W/m^2 to 1300 W/m^2 (e.g. 3.25 times). Of course, the lowering of the ionic conductivity of the electrolyte has the effect of increasing the ohmic resistance of the cell (poor ionic conduction in the electrolyte). Furthermore, the slopes of the curves of the power density vs current density is sharp from an ionic conductivity at least of 2.65 S/m. Accordingly a high power density is obtained with a small variation of the current density if the ionic conductivity is very high. It is also noted that the drop in performance of the cell is not significant when the conductivity of the electrolyte decreases from 265 S/m to 26.5 S/m. Thus, operating the cell with an electrolyte conductivity of 26.5 S/m will cause significant losses in power density than operating it with an electrolyte conductivity of 265 S/m.

Fig. 3 shows the effect of Ni electrical conductivity on cell performance. Thus, by decreasing the electrical conductivity from 2500 S/m to 2.5 S/m (3 orders of magnitude), a drop from 1400 W/m^2 to 1100 W/m^2 (a ratio of 1.3) in performance of the cell is observed. This drop is less important than that observed for the effect of the ionic conductivity of the electrolyte where a 3.5 times drop in power density is observed when the conductivity decreases from 265 S/m to 0.265 S/m.

Nevertheless, the curves in Fig. 3 show that the variation of the power density curves as a function of the current for a conductivity of nickel which varies between 2500 S/m and 250 S/m are almost identical and the decrease in performance of the cell is not significant between 250 S/m and 25 S/m. This indicates that for a material having a conductivity of 25 S/m the MC-LFC stack would still offer good performance.

The increase in the electrical conductivity of the cathode layer from 1.9 S/m to 60 S/m (a ratio of 31.6 between the highest and the lowest cathode conductivity) has a very significant positive effect on the performance of the cell (Fig. 4).The ratio of the power density at 60 S/m (almost 2000 W/m^2) and that at 1.9 S/m (1400 W/m^2) is 1.4. in a 3 orders (1000 times) magnitude variation in the anode conductivity, an improvement of 1.3 times was observed in the power density of the cell whereas for a variation of 31.6 times in the cathode conductivity, an improvement in of 1.4 times in the power density of the MC-LFC is observed. The contribution of the cathode conductivity variation in cell power density improvement is significantly higher than those of the anode. Due to the difference of magnitudes in the variation of the electrolyte ionic conductivity (1000 times) and that for the cathode conductivity (31.6 times), we might point out that the 3.5 times of power density improvement due to electrolyte conductivity improvement is less than those of 1.4-time improvement in the power density due to the variation of cathode conductivity. One might think that the cathode material, where the electrons are consumed in the oxygen reduction reactions (see above reaction R5), is the limiting factor of the MC-LFC cell performance. However, the electrical conductivity of the materials cannot be the only parameter to be considered. Admittedly, a greater conductivity of the electrodes and of the electrolyte favors the conduction of the current, which reduces the ohmic losses and significantly increases the performance of the cell.

Other operating parameters as the increase in the temperature may have a positive impact in the electrolyte ionic conductivity and the species diffusion coefficient which may also increase. But the performance of the MC-LFC cell decreases when the temperature increases (Fig. 5). This is probably due to the decrease in current densities (Eq. 9 and Eq.14) probably caused by parasitic reactions. Indeed, the decrease in the power density of the MC-LFC when the operating temperature increases is probably due to a high entropy of reaction due to the parasitic reactions. This means that at a constant reaction rate, the parasitic reactions increase with the temperature causing more entropy production. This increase in entropy production causes a decrease in the production of electrical power. Contrary to the temperature, the increase in the operating pressure (Fig. 6) leads to an increase in both the chemical potentials (molar free enthalpies) of the various reagents reactions and the associated current density of their electrodes reactions of the MC-LFC cell, and therefore the power (or the electrical energy) produced increases. The variation of operating pressure of the MC-LFC from 1 atm to 10 atm, enhances significantly the power density of approximately 500 W/m^2 .

Fig. 7 and Fig.8 show, respectively, the variation of the power density with the exchange current density of the anode or cathode reactions of the MC-LFC stack. For an increase in 2 orders of magnitude (e.g.from 0.0075 A.cm^{-2} to 0.75 A.cm^{-2}) of the anodic current density, the power density increases 1.7 time (e.g. from 1400 W/m^2 to 2400 W/m^2). The increase of the power density is only 1.2 time when the exchange anodic current density increases one order on magnitude from 0.075 A.cm^{-2} to 0.75 A.cm^{-2}. This an indication that even if the anodic exchange current density is increased to 3 orders of magnitude, the power density will probably not increase to more than 2 times. Thus the contribution of the anodic reaction exchange current density in the improvement of the cell power density is less important than that of the MC-LFC electrolyte ionic conductivity. Fig.8 shows that even with a 5 orders of magnitude in the increase of the cathode reaction exchange current density, the increase in the power density is less than 10% (a ratio of 1.08 for an increase in cathode current density from 0.158 S/m to 15 800 S/m)

We can point out that the exchange current density is one of the important practical electrochemical parameter which probes the kinetic reactions of the redox reactions at the interface of the anode/electrolyte or cathode/electrolyte of MC-LFC unit. Accordingly, its values depend on the redox type reactions but also on the nature and surface state of the electrodes. In this work, the simulation was made on only nickel anode and nickel oxide cathode. Thus, the results may be improve if we perform the simulation on other type of anode and cathode materials or if we increase their active surface area.

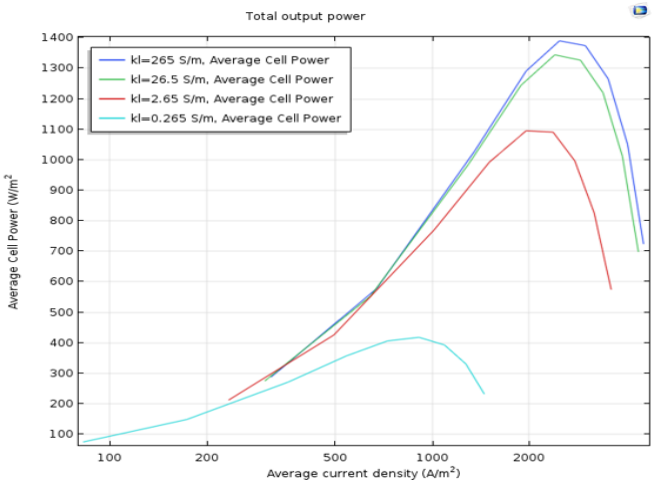

Figure 2. Influence of electrolyte conductivity on the output power density of the MC-LFC stack

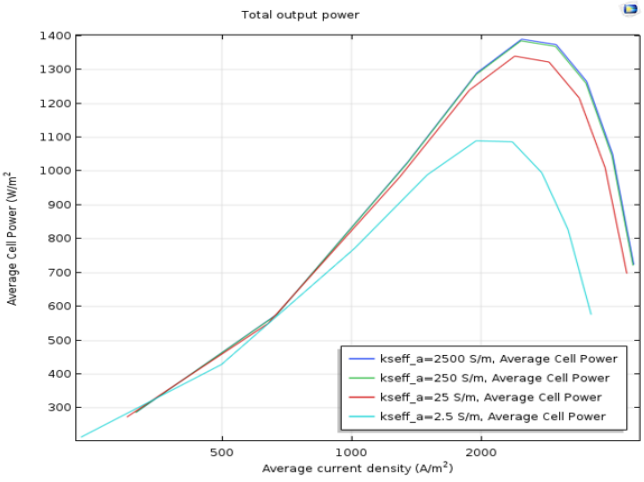

Figure 3. Influence of the electrical conductivity of the anode material (Ni) on the output power density of the MC-LFC stack

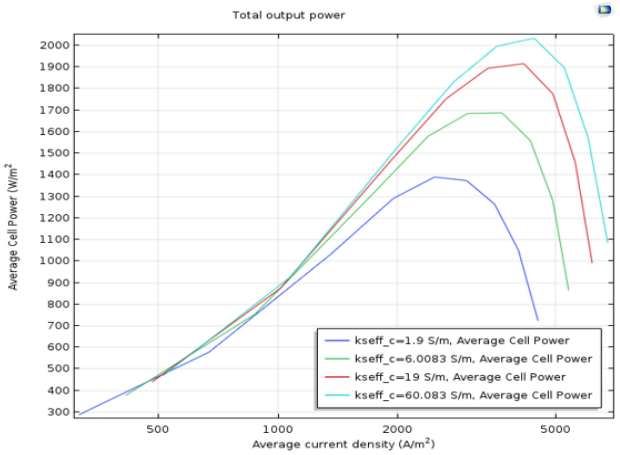

Figure 4. Influence of the electrical conductivity of the cathode material (Ni) on the output power density of the MC-LFC stack

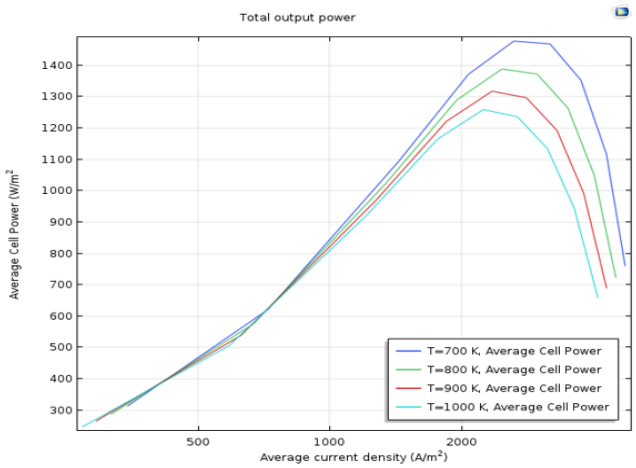

Figure 5. Influence of the operating temperature on the output power density of the MC-LFC stack

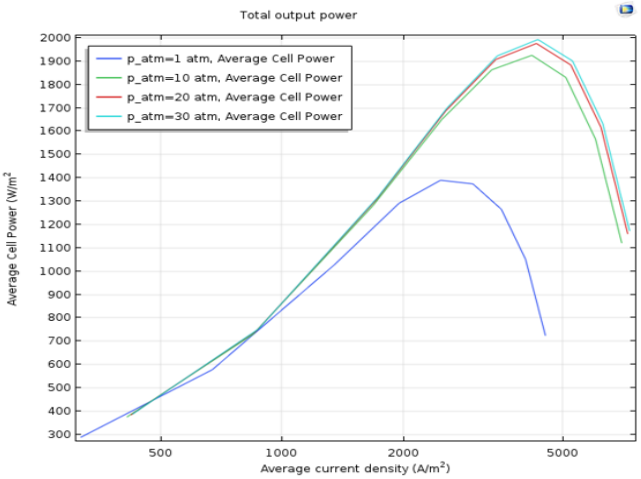

Figure 6. Influence of the operating cell pressure on the output power density of the MC-LFC stack

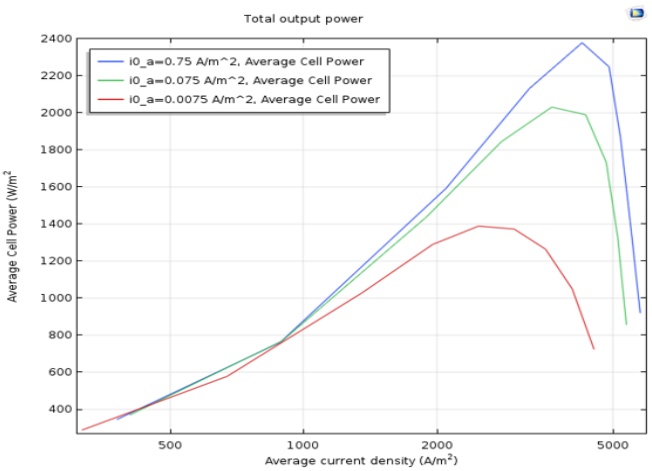

Figure 7. Influence of the anodic exchange current density on the output power density of the MC-LFC stack

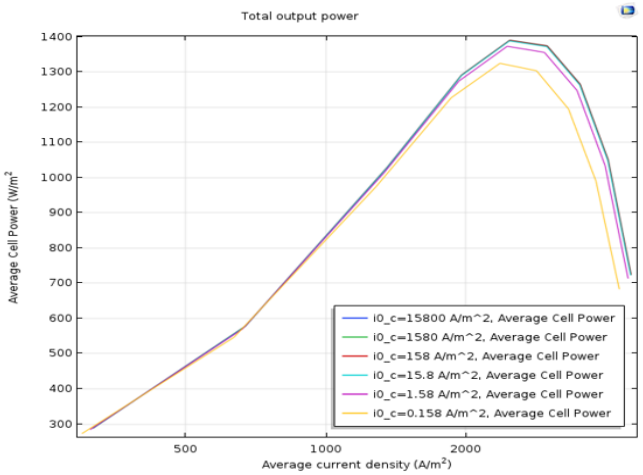

Figure 8. Influence of the cathodic exchange current density on the output power density of the MC-LFC stack

The cathode reactions R5 show clearly the concentration of O_2 and CO_2 might have an impact on the variation of the power density with the current density. Fig. 9 and Fig. 10 show, respectively, the effect of the variation of the molar concentrations of CO_2 and O_2 on the performance of the cell.

Increasing the molar concentration of CO_2 from 1 mol/m^3 to 5 mol/m^3 decreases the maximum power density of the cell by more than 50 W/m^2 (Fig. 9). This can be related to a diffusion limiting process of the CO_2 reduction. The rate of reduction of CO_2 is less than the concentration of CO_2 arriving at the electrode surface. This can be related to a limited active surface area or active states at the NiO cathode electrode surface. Electrode surface engineering which may help to increase the active surface area or active would the appropriate approach to overcome this limitation.

Similar results are obtained for the reduction of O_2. Increasing the concentration of O_2 (Fig. 10) causes a reduction in the power density of the cell. As for the CO2 reduction, this can be related to a diffusion limiting process of the O_2 reduction or to a limited active surface area or active states at the NiO cathode electrode surface. The drop in performance is less important in comparison to that of CO_2. This indicates that the O_2 reduction is more facilitate than that of CO_2 on the NiO

surface. Development of mixed or bi-functional catalysts is underway and will help to understand the role of the electrode materials in the reduction of CO_2 and O_2 respectively.

Based on the effect of the CO_2 and O_2 concentrations on the cell power density, for the cell to deliver maximum output power (above 1400 W/m^2), the concentration of O_2 and CO_2 in the cathode compartment must be controlled respectively to values less than 10 mol/m^3 and 5 mol /m^3).

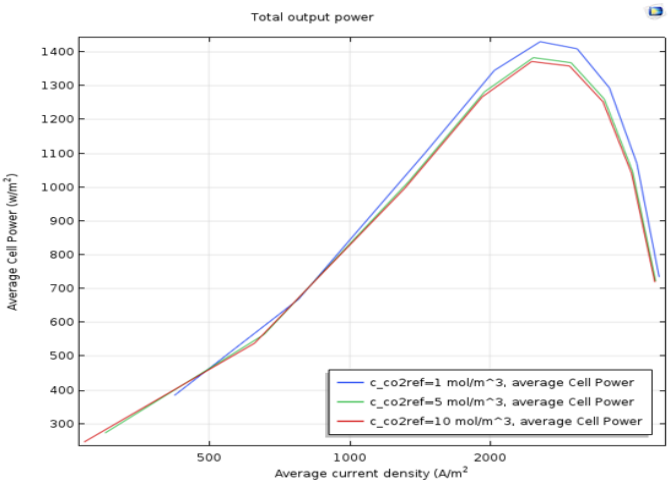

Figure 9. Influence of the molar concentration of the cathode inlet gas CO_2 on the output power density of the MC-LFC stack.

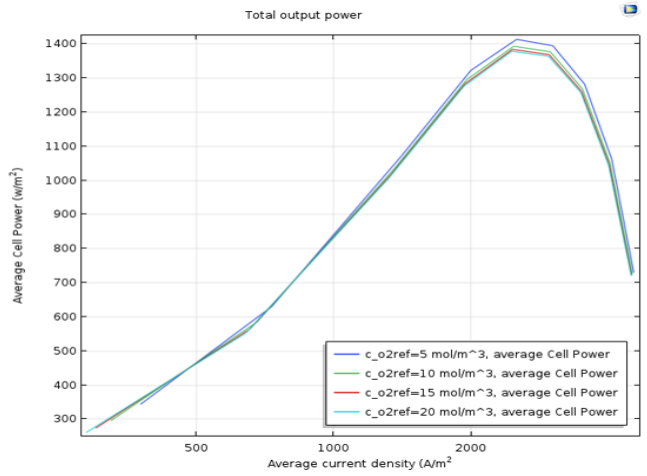

Figure 10. Influence of the molar concentration of the cathode inlet gas O_2 on the output power density of the MC-LFC stack

It is true that the increase in the concentration of CO_2 decreases the performance of the cell. However, the low electrical conductivity of the cathode material (NiO) is the most limiting parameter. It is then crucial to choose cathode materials having a higher and stable conductivity in the molten carbonate $(LiNaCs)_2CO_3$ to further improve the performance of the MC-LFC cell. decreases the rate at which the gases formed can reach the electrode/electrolyte interface so that the R2, R3 and R4 reactions can occur.

4. CONCLUSIONS

Based on the results obtained in this wok on the MC-LFC cell developed using COMSOL software, it can be concluded that:

1) The optimum power density obtained in this model (1400 W/m^2) agrees with other values different approaches, electrodes, temperature range (temperature is lower than in other studies), fuel and electrolyte.

2) This cell model is based on a nickel anode and a nickel oxide cathode and a green carbon precursor biopolymer (lignin) was the fuel;

3) The data obtained for modelling MC-LFC cells using similar operating conditions were compared to the experimental data of DCFC cells except for the case of the SOFC stack operating around 850 °C;

4) In general, the simulated curves based on the variation of the power density with the current density show a maximum power density of 1390 W/m^2. It is noted that the smallest value of the maximum power density obtained according to the experimental data is 250 W/m^2 and the largest is 2250 W/m^2. Accordingly, the results obtained from modeling agree with the experimental results. The results of the model are coherent and can be considered as being reliable.

5) The results of the models also show that an increase of the cell temperature or on the CO_2 concentration at the cathode has a negative effect on the cell performance. On the contrary, an increase of the pressure, or of the exchange current densities of the anode, the cathode reactions or the conductivity of the electrolyte contribute to the improvement of the cell performances.

REFERENCES

[1] Brouwer, J., Jabbari, F., Leal, E. M., & Orr, T. (2005). Analysis of a molten carbonate fuel cell: Numerical modeling and experimental validation. Journal of Power Sources, 158(1), 213-224. https://doi.org/10.1016/j.jpowsour.2005.07.093

[2] Srinivasan, S Fuel cells: from fundamentals to applications: Springer Science & Business media, 2006.

[3] Kordesch, K. V., & Simader, G. R. (1995). Environmental impact of fuel cell technology. Chemical Reviews, 95(1), 191-207.

[4] Lima, R. B., Raza, R., Qin, H., Li, J., Lindström, M. E., & Zhu, B. (2013). Direct lignin fuel cell for power generation. RSC advances, 3(15), 5083-5089 https://doi.org/10.1039/C3RA23418E.

[5] Zhao, X., & Zhu, A. J. (2016). Efficient conversion of lignin to electricity using a novel direct biomass fuel cell mediated by polyoxometalates at low temperatures. ChemSusChem, 9(2), 197-207 https://doi.org/10.1002/cssc.201501446.

[6] Wu, W., Zhang, Y., Ding, D., & He, T. (2018). A high‐performing direct carbon fuel cell with a 3D architectured anode operated below 600 C. Advanced Materials, 30(4), 1704745 https://doi.org/10.1002/adma.201704745.

[7] Cao, D., Sun, Y., & Wang, G. (2007). Direct carbon fuel cell: fundamentals and recent developments. Journal of Power Sources, 167(2), 250-257 https://doi.org/10.1016/j.jpowsour.2007.02.034.

[8] Jiang, C., Ma, J., Bonaccorso, A. D., & Irvine, J. T. (2012). Demonstration of high power, direct conversion of waste-derived carbon in a hybrid direct carbon fuel cell. Energy & Environmental Science, 5(5), 6973-6980 DOI: 10.1039/C2EE03510C.

[9] Al-Hamed, K. H. M., & Dincer, I. (2020). A novel integrated solid-oxide fuel cell powering system for clean rail applications. Energy Conversion and Management, 205, 112327 https://doi.org/10.1016/j.enconman.2019.112327.

[10] Wu, H., Xiao, J., Zeng, X., Li, X., Yang, J., Zou, Y., ... & Liu, J. (2019). A high performance direct carbon solid oxide fuel cell–A green pathway for brown coal utilization. Applied Energy, 248, 679-687 https://doi.org/10.1016/j.apenergy.2019.04.104.

[11] Demirdoven, N., & Deutch, J. (2004). Hybrid cars now, fuel cell cars later. Science, 305(5686), 974-976 DOI: 10.1126/science.1093965.

[12] Jacques, W. (1896). Method of converting potential energy of carbon into electrical energy, US Patent 555,511.

[13] Cooper, J. F., & Selman, R. (2009). Electrochemical oxidation of carbon for electric power generation: a review. ECS Transactions, 19(14), 15 DOI 10.1149/1.3220176.

[14] Giddey, S., Badwal, S. P. S., Kulkarni, A., & Munnings, C. (2012). A comprehensive review of direct carbon fuel cell technology. Progress in Energy and Combustion Science, 38(3), 360-399 https://doi.org/10.1016/j.pecs.2012.01.003.

[15] Rady, A. C., Giddey, S., Badwal, S. P., Ladewig, B. P., & Bhattacharya, S. (2012). Review of fuels for direct carbon fuel cells. Energy & Fuels, 26(3), 1471-1488 https://doi.org/10.1021/ef201694y.

[16] Gür, T. M. (2010). Mechanistic modes for solid carbon conversion in high temperature fuel cells. Journal of The Electrochemical Society, 157(5), B751 DOI 10.1149/1.3357050.

[17] Gür, T. M. (2013). Critical review of carbon conversion in "carbon fuel cells". Chemical reviews, 113(8), 6179-6206 https://doi.org/10.1021/cr400072b.

[18] Zhou, W., Jiao, Y., Li, S. D., & Shao, Z. (2016). Anodes for Carbon‐Fueled Solid Oxide Fuel Cells. ChemElectroChem, 3(2), 193-203 https://doi.org/10.1002/celc.201500420.

[19] Cao, T., Huang, K., Shi, Y., & Cai, N. (2017). Recent advances in high-temperature carbon–air fuel cells. Energy & Environmental Science, 10(2), 460-490 DOI: 10.1039/C6EE03462D

[20] Zecevic, S., Patton, E. M., & Parhami, P. (2004). Carbon–air fuel cell without a reforming process. Carbon, 42(10), 1983-1993 https://doi.org/10.1016/j.carbon.2004.03.036.

[21] Jiang, C., Ma, J., Corre, G., Jain, S. L., & Irvine, J. T. (2017). Challenges in developing direct carbon fuel cells. Chemical Society Reviews, 46(10), 2889-2912 DOI: 10.1039/C6CS00784H.

[22] Fuente-Cuesta, A., Jiang, C., Arenillas, A., & Irvine, J. T. (2016). Role of coal characteristics in the electrochemical behaviour of hybrid direct carbon fuel cells. Energy & Environmental Science, 9(9), 2868-2880 DOI: 10.1039/C6EE01461E.

[23] Li, S., Pan, W., Wang, S., Meng, X., Jiang, C., & Irvine, J. T. (2017). Electrochemical performance of different carbon fuels on a hybrid direct carbon fuel cell. international journal of hydrogen energy, 42(25), 16279-16287 https://doi.org/10.1016/j.ijhydene.2017.05.150.

[24] Kouchachvili, L., & Ikura, M. (2011). Performance of direct carbon fuel cell. International journal of hydrogen energy, 36(16), 10263-10268 https://doi.org/10.1016/j.ijhydene.2010.10.036.

[25] Vutetakis, D. G., Skidmore, D. R., & Byker, H. J. (1987). Electrochemical oxidation of molten carbonate‐coal slurries. Journal of the electrochemical society, 134(12), 3027 DOI 10.1149/1.2100334.

[26] Jiang, C., & Irvine, J. T. (2011). Catalysis and oxidation of carbon in a hybrid direct carbon fuel cell. Journal of Power Sources, 196(17), 7318-7322 https://doi.org/10.1016/j.jpowsour.2010.11.066.

[27] Tanimoto, K., Miyazaki, Y., Yanagida, M., Tanase, S., Kojima, T., Ohtori, N., ... & Kodama, T. (1992). Cell performance of molten-carbonate fuel cell with alkali and alkaline-earth carbonate mixtures. Journal of power sources, 39(3), 285-297 https://doi.org/10.1016/0378-7753(92)80002-S.

[28] Nabae, Y., Pointon, K. D., & Irvine, J. T. (2008). Electrochemical oxidation of solid carbon in hybrid DCFC with solid oxide and molten carbonate binary electrolyte. Energy & Environmental Science, 1(1), 148-155 DOI: 10.1039/B804785E.

[29] Xu, X., Zhou, W., & Zhu, Z. (2014). Stability of YSZ and SDC in molten carbonate eutectics for hybrid direct carbon fuel cells. Rsc Advances, 4(5), 2398-2403 DOI: 10.1039/C3RA46600K.

[30] Chen, C., Tran, T., Olivares, R., Wright, S., & Sun, S. (2014). Coupled experimental study and thermodynamic modeling of melting point and thermal stability of Li2CO3-Na2CO3-K2CO3 based salts. Journal of solar energy engineering, 136(3) https://doi.org/10.1115/1.4027264.

[31] Janz, G. J., Allen, C. B., Downey Jr, J. R., & Tomkins, R. (1976). EUTECTIC DATA: safety, hazards, corrosion, melting points, compositions, and bibliography (No. TID-27163-P2). Rensselaer Polytechnic Inst., Troy, NY (USA). Cogswell Lab, DOE:PO-WA-76-4280

[32] Morita, H., Kawase, M., Mugikura, Y., & Asano, K. (2010). Degradation mechanism of molten carbonate fuel cell based on long-term performance: long-term operation by using bench-scale cell and post-test analysis of the cell. Journal of Power Sources, 195(20), 6988-6996 https://doi.org/10.1016/j.jpowsour.2010.04.084.

[33] McKee, D. W., & Chatterji, D. (1975). The catalytic behavior of alkali metal carbonates and oxides in graphite oxidation reactions. Carbon, 13(5), 381-390 https://doi.org/10.1016/0008-6223(75)90006-8.

[34] Glugla, P. G., & De Carlo, V. J. (1982). The specific conductance of molten carbonate fuel cell tiles. J. Electrochem. Soc.;(United States), 129(8) https://doi.org/10.1149/1.2124263.

[35] Lee, E. K., Park, S. A., Jung, H. W., & Kim, Y. T. (2018). Performance enhancement of molten carbonate-based direct carbon fuel cell (MC-DCFC) via adding mixed ionic-electronic conductors into Ni anode catalyst layer.

Journal of Power Sources, 386, 28-33 https://doi.org/10.1016/j.jpowsour.2018.01.078.
[36] Hao, W. B., He, X. J., & Mi, Y. L. (2014), "Achieving high performance in intermediate temperature direct carbon fuel cells with renewable carbon as a fuel source," Appl. Energy, vol. 135, p. 174-181, Dec 2014 https://doi.org/10.1016/j.apenergy.2014.08.055.
[37] Lee, J. Y., Song, R. H., Lee, S. B., Lim, T. H., Park, S. J., Shul, Y. G., & Lee, J. W. (2014). A performance study of hybrid direct carbon fuel cells: Impact of anode microstructure. International journal of hydrogen energy, 39(22), 11749-11755 https://doi.org/10.1016/j.ijhydene.2014.05.145
[38] Hao, W., & Mi, Y. (2016). A direct carbon fuel cell with a CuO–ZnO–SDC composite anode. RSC advances, 6(55), 50201-50208. doi: 10.1039/C6RA04949D.
[39] Liu, J., Yuan, H., Qiao, J., Feng, J., Xu, C., Wang, Z. & Sun, K. (2017). Hierarchical hollow nanofiber networks for high-performance hybrid direct carbon fuel cells. Journal of Materials Chemistry A, 5(33), 17216-17220 DOI: 10.1039/C7TA04616B.
[40] Tomellini, M. (1988). X-ray photoelectron spectra of defective nickel oxide. Journal of the Chemical Society, Faraday Transactions 1: Physical Chemistry in Condensed Phases, 84(10), 3501-3510.
[41]. Zhao . L & Zhu, Q.-s. "Novel Cathode Material for Direct Carbon Fuel Cell," vol. 6, no. 5, p. 822, 2006.
[42] Li, S., Jiang, C., Liu, J., Tao, H., Meng, X., Connor, P., ... & Irvine, J. T. (2018). Mechanism of enhanced performance on a hybrid direct carbon fuel cell using sawdust biofuels. Journal of Power Sources, 383, 10-16 https://doi.org/10.1016/j.jpowsour.2018.02.040.
[43] Lima, R. B., Raza, R., Qin, H., Li, J., Lindström, M. E., & Zhu, B. (2013). Direct lignin fuel cell for power generation. RSC advances, 3(15), 5083-5089 DOI: 10.1039/C3RA23418E.
[44] Thakur, V. K., Thakur, M. K., Raghavan, P., & Kessler, M. R. (2014). Progress in green polymer composites from lignin for multifunctional applications: a review. ACS Sustainable Chemistry & Engineering, 2(5), 1072-1092 https://doi.org/10.1021/sc500087z.
[45] G. Sarlos, P.-A. Haldi e& P. Verstraete, Systèmes énergétiques: Offre et demande d'énergie: méthodes d'analyse vol. 21: PPUR presses polytechniques, 2003.
[46] Kornhauser, A. A. & Agarwal, Q.-s. R. "Modeling and Design for a Direct Carbon Fuel Cell with Entrained Fuel and Oxidizer," Virginia Polytechnic Institute and State University (US), 2005 https://doi.org/10.2172/839468.
[47] Liu, Q., Tian, Y., Xia, C., Thompson, L. T., Liang, B., & Li, Y. (2008). ‘’Modeling and simulation of a single direct carbon fuel cell’’. Journal of Power Sources, 185(2), 1022-1029 https://doi.org/10.1016/j.jpowsour.2008.08.100
[48] Tare, V. B., & Wagner Jr, J. B. (1983). ‘’Electrical conductivity in two phase nickel–nickel oxide mixtures and conductivity of nickel oxide at the nickel–nickel oxide phase boundary. Journal of applied physics’’, 54(11), 6459-6462 https://doi.org/10.1063/1.331927.
[49] Kojima, T., Miyazaki, Y., Nomura, K., & Tanimoto, K. (2008). Density, surface tension, and electrical conductivity of ternary molten carbonate system Li2CO3–Na2CO3–K2CO3 and methods for their estimation. Journal of the Electrochemical Society, 155(7), F150 DOI 10.1149/1.2917212.
[50] Fuller, E. N., Schettler, P. D., & Giddings, J. C. (1966). ‘’New method for prediction of binary gas-phase diffusion coefficients. Industrial & Engineering Chemistry’’, 58(5), 18-27.
[51] T. Fujii, Theory of laminar film condensation: Springer Science & Business Media, 2012.
[52] Touloukian, Y. S., Saxena, S. C., & Hestermans, P. (1975). Thermophysical Properties of Matter, Vol. 11: Viscosity. IFI/Plenum.
[53] I. Dinčer et M. Kanoğlu, "Appendix B: Thermophysical Properties," dans Refrigeration Systems and Applications (2nd Edition): John Wiley & Sons, p. 433.
[54] Pramuanjaroenkij, Kakaç, A. S. & Zhou, X. Y. "Mathematical analysis of planar solid oxide fuel cells," dans Mini-Micro Fuel Cells: Springer, 2008, p. 359-390 DOI: 10.1007/978-1-4020-8295-5_24.
[55] White, F. "Fluid mechanics/Frank M. White," éd: McGraw-hill, 2003.
[56] U, H. and Kee, R. J. , (2008). "Modeling distributed charge-transfer processes in SOFC membrane electrode assemblies." Journal of the Electrochemical Society 155(7): B715 DOI 10.1149/1.2913152.
[57] Daneshvar, Keyvan., Dotelli, Giovanni., Cristiani, Cinzia., Pelosato, Renato., & Santarelli, Massimo. (2014). Modeling and parametric study of a single solid oxide fuel cell by finite element method. Fuel Cells, 14(2), 189-199 https://doi.org/10.1002/fuce.201300235.
[58] Elleuch, A., Boussetta, A., & Halouani, K. (2012). Analytical modeling of electrochemical mechanisms in CO2 and CO/CO2 producing Direct Carbon Fuel Cell. Journal of Electroanalytical Chemistry, 668, 99-106 https://doi.org/10.1016/j.jelechem.2012.01.010.
[59] Subramanian, N., Haran, B. S., Ganesan, P., White, R. E., & Popov, B. N. (2002). Analysis of molten carbonate fuel cell performance using a three-phase homogeneous model. Journal of the Electrochemical Society, 150(1), A46 DOI 10.1149/1.1522721.
[60] Snoeck, J. W., Froment, G. F., & Fowles, M. (2002). Steam/CO2 reforming of methane. Carbon filament formation by the Boudouard reaction and gasification by CO2, by H2, and by steam: kinetic study. Industrial & engineering chemistry research, 41(17), 4252-4265 https://doi.org/10.1021/ie010666h.
[61] Hemmes, K., & Cassir, M. (2011). A theoretical study of the carbon/carbonate/hydroxide (electro-) chemical system in a direct carbon fuel cell. Journal of Fuel Cell Science and Technology, 8(5) https://doi.org/10.1115/1.4003750.
[62] Nakagawa, N., & Ishida, M. (1988). Performance of an internal direct-oxidation carbon fuel cell and its evaluation by graphic exergy analysis. Industrial & engineering chemistry research, 27(7), 1181-1185.
[63] Aloui, T., & Halouani, K. (2007). Analytical modeling of polarizations in a solid oxide fuel cell using biomass syngas product as fuel. Applied Thermal Engineering, 27(4), 731-737 https://doi.org/10.1016/j.applthermaleng.2006.10.011.
[64] Bird, R. B. (2002). Transport phenomena. Appl. Mech. Rev., 55(1), R1-R4.
[65] Soulaïmani, A., & Fortin, M. (1994).Finite element solution of compressible viscous flows using

conservative variables. Computer methods in applied mechanics and engineering, 118(3-4), 319-350 https://doi.org/10.1016/0045-7825(94)90006-X.

[66] Wesselingh, J. A., & Krishna, R. (2000). Mass transfer in multicomponent mixtures, Vol. 203. Delft: Delft University Press.

[67] Tjaden, B., Cooper, S. J., Brett, D. J., Kramer, D., & Shearing, P. R. (2016). On the origin and application of the Bruggeman correlation for analysing transport phenomena in electrochemical systems. Current opinion in chemical engineering, 12, 44-51 https://doi.org/10.1016/j.coche.2016.02.006.

[68] Nield, D. A. & Bejan A., Convection in porous media vol. 3: Springer, 2006.
https://doi.org/10.1007/978-3-319-49562-0.

[69] Le Bars, M., & Worster, M. G. (2006). Interfacial conditions between a pure fluid and a porous medium: implications for binary alloy solidification. Journal of Fluid Mechanics, 550, 149-173: https://doi.org/10.1017/S0022112005007998.

[70] Carrier III, W. D. (2003). Goodbye, hazen; hello, kozeny-carman. Journal of geotechnical and geoenvironmental engineering, 129(11), 1054-1056 https://doi.org/10.1061/(ASCE)1090-0241(2003)129:11(1054).

[71] LaMarche, C. Q., Curtis, J. S., & Metzger, P. T. (2011). Permeability of JSC-1A: A lunar soil simulant. Icarus, 212(1), 383-389 https://doi.org/10.1016/j.icarus.2010.12.015.

[72] Carman PC. Flow of Gases Through Porous Media. London: Butterworth Publications; 1956

[73] Lair, V., Albin, V., Ringuedé, A., & Cassir, M. (2012). Theoretical predictions vs. experimental measurements of the electrical conductivity of molten Li2CO3–K2CO3 modified by additives. international journal of hydrogen energy, 37(24), 19357-19364 https://doi.org/10.1016/j.ijhydene.2011.09.153.

[74] Janz, G. J. (1988). Thermodynamic and transport properties for molten salts: correlation equations for critically evaluated density, surface tension, electrical conductance, and viscosity data. Journal of physical and chemical reference data, 17.

[75] Gaillard, F., Malki, M., Iacono-Marziano, G., Pichavant, M., & Scaillet, B. (2008). Carbonatite melts and electrical conductivity in the asthenosphere. Science, 322(5906), 1363-1365 DOI: 10.1126/science.1164446.

[76] Kojima, T. (2009). Physical and chemical properties of molten carbonates. Disertation. Kobe University Graduate School of Natural Science and Technology.

[77] Kojima, T., Miyazaki, Y., Nomura, K., & Tanimoto, K. (2007). Electrical conductivity of molten Li2CO3–X2CO3 (X: Na, K, Rb, and Cs) and Na2CO3–Z2CO3 (Z: K, Rb, and Cs). Journal of The Electrochemical Society, 154(12), F222 DOI 10.1149/1.2789389.

[78] Kojima, T., Yanagida, M., Tanimoto, K., Tamiya, Y., Matsumoto, H., & MiyazakI, Y. (1999). The surface tension and the density of molten binary alkali carbonate systems. Electrochemistry, 67(6), 593-602 https://doi.org/10.5796/electrochemistry.67.593.

[79] Rosen, J., Geary, T., Hilmi, A., Blanco-Gutierrez, R., Yuh, C. Y., Pereira, C. S., ... & Barckholtz, T. A. (2020). Molten carbonate fuel cell performance for CO2 capture from natural gas combined cycle flue gas. Journal of the Electrochemical Society, 167(6), 064505 DOI 10.1149/1945-7111/ab7a9f.